

Improved laser-induced forward transfer of organic semiconductor thin films by reducing the environmental pressure and controlling the substrate–substrate gap width

James Shaw-Stewart · Bryan Chu · Thomas Lippert ·
Ylenia Maniglio · Matthias Nagel · Frank Nüesch ·
Alexander Wokaun

Received: 3 June 2011 / Accepted: 24 August 2011 / Published online: 23 September 2011
© Springer-Verlag 2011

Abstract Laser-induced forward transfer (LIFT) has been investigated for bilayer transfer material systems: silver/organic film (Alq_3 or PFO). The LIFT process uses an intermediate dynamic release layer of a triazene polymer. This study focuses on the effect of introducing a controlled donor–receiver substrate gap distance and the effect of doing the transfer at reduced air pressures, whilst varying the fluence up to $\sim 200 \text{ mJ/cm}^2$. The gap between ‘in-contact’ substrates has been measured to be a minimum of $2\text{--}3 \mu\text{m}$. A linear variation in the gap width from ‘in contact’ to $40 \mu\text{m}$ has been achieved by adding a spacer at one side of the substrate–substrate sandwich. At atmospheric pressure, very little transfer is achieved for Alq_3 , although PFO shows some signs of successful *doughnut* transfer (with a large hole in the middle) in a narrow fluence range, at gaps greater than $20 \mu\text{m}$. For the transfer of Ag/PFO bilayers at atmospheric pressure, the addition of a PFO layer onto the receiver substrate improved the transfer enormously at smaller gaps and higher fluences. However, the best transfer results were obtained at reduced pressures where a 100% transfer success rate is obtained within a certain fluence window. The quality of the pixel morphology at less than 100 mbar is much higher than at atmospheric pressure, particularly when

the gap width is less than $20 \mu\text{m}$. These results show the promise of LIFT for industrial deposition processes where a gap between the substrates will improve the throughput.

1 Introduction

Early laser-based material transfer was carried out as long ago as 1970 on ink [1] and was followed by the transfer of metals using a similar technique in the 1980s [2]. These experiments marked the precursor to laser-induced forward transfer (LIFT), which has been subsequently improved with the use of an absorbing intermediate layer. LIFT is now used for the transfer of complex functional materials [3, 4]. Recently, research into LIFT has intensified and various different materials have been transferred including microorganisms [5], biological cells [6], biomolecule solutions [7], quantum dots [8], organic light-emitting diodes (OLEDs) [9], organic thin-film transistors [10], ceramics [11], 3-D interconnects [12], polystyrene microbeads [13], polymeric sensors [14], and liposomes [15]. Many of these breakthroughs used an absorbing intermediate layer, termed the dynamic release layer (DRL). The DRL is often an inorganic thermal absorber, such as titanium [16], or a polymer that breaks down in a photon-induced chemical reaction, such as the class of triazene polymers [17].

LIFT for the fabrication of polymeric OLEDs (PLEDs) has already been investigated [9, 17]. The observations from those studies included good functionality of the transferred devices, different transfer qualities onto different receiver substrates, and also some minor cracking within the pixel. Overall, the process looked a success, but one feature appeared undesirable: the pressing of the substrates together ‘in contact’. There were two distinct disadvantages to this on the laboratory scale. Firstly, transfer ‘in contact’ often

J. Shaw-Stewart (✉) · B. Chu · Y. Maniglio · M. Nagel · F. Nüesch
Laboratory for Functional Polymers, Empa Swiss Federal Laboratories for Materials Science and Technology, Überlandstrasse 129, 8600 Dübendorf, Switzerland
e-mail: james.shaw-stewart.2004@pem.cam.ac.uk

J. Shaw-Stewart · T. Lippert · A. Wokaun
Materials Group, General Energies Department, Paul Scherrer Institut, 5232 Villigen-PSI, Switzerland

T. Lippert
e-mail: thomas.lippert@psi.ch

caused the pixel to adhere to both the donor substrate and the receiver substrate after the laser ablation. This meant that separating the substrates was crucial to successful deposition. The second problem was that ‘in contact’ is not actually in contact. A small gap of some width must be present, and the problem of a single dust particle ruining the transfer by increasing this gap width was observed. In addition, shadowgraphy experiments have shown the generation of a considerable shock wave at atmospheric pressure [18–20]. Reduced pressure and transfer across large gap widths (0.5 and 1 mm) have both already been investigated using shadowgraphy [19]. That investigation showed the effect of the reflected shock wave in destroying the flyers at atmospheric pressure. It also showed that the transfer was unsuccessful at reduced pressures, because the flyers either folded too much at low fluences or were destroyed on impact at higher fluences.

In this study the effect of different gap widths of up to 40 μm has been investigated at atmospheric pressure and at reduced pressures, for the LIFT setup shown in Fig. 1. We have successfully transferred bilayer thin-film pixels across a gap. The main previous investigation used much larger gaps than we have used here (500 vs. 40 μm) [19]. The larger gap, along with the lack of coating on the glass receiver substrate, may explain why the transfer was not successful previously, but has been successfully achieved across a gap in this study. Previous observations of the destructive nature of the shock wave at atmospheric pressure [19] have been reaffirmed, and the benefit of reducing the air resistance, and the shock wave, by reducing the pressure further supports this observation. The recent observation that the transfer depended on the receiver substrate [17] has also been followed up by adding a layer of the organic material used in the transfer onto the receiver substrate to improve the pixel–receiver substrate adhesion at atmospheric pressures.

The DRL material in this study is a triazene polymer (TP) with the chemical structure shown in Fig. 2a. The metal used is silver, a standard electrode material for OLEDs, including the very first OLED devices in 1987 [21]. The first OLEDs were made with an electroluminescent layer of Alq₃ (aluminium tri-8-hydroxyquinoline, shown in Fig. 2b). Alq₃ is a small molecule and has already been a material of interest for OLED transfer [16]. Our previous investigations into PLEDs have focussed on MEH-PPV (poly[2-methoxy, 5-(2-ethylhexyloxy)-1,4-phenylene vinylene]) [9, 17, 19]. However, in this study we have changed our conjugated polymer of interest to PFO (poly[9,9-dioctylfluorene-2,7-diyl] shown in Fig. 2c). PFO is used variously as a blue emitter, a host for phosphorescent dyes, and a starting point for more complex homo- and copolymers [22]. We have also observed PFO to have better spin-coated film formation properties than MEH-PPV.

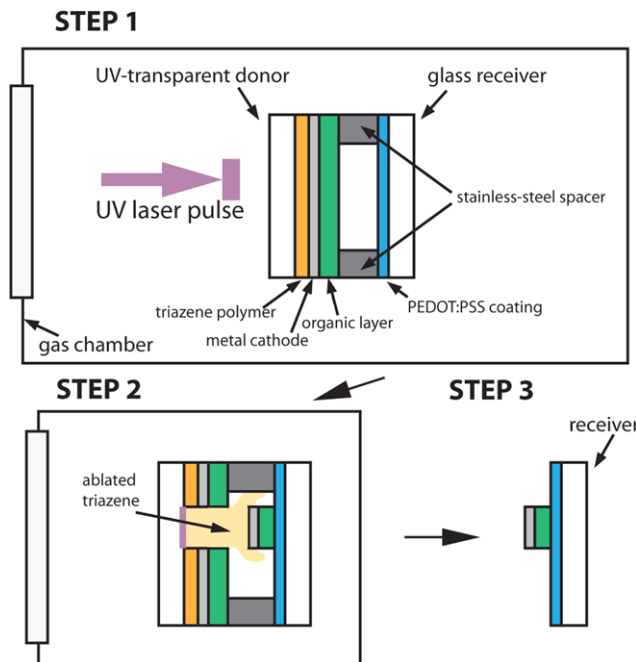


Fig. 1 A schematic outlining the LIFT process, as detailed in the paper: *Step 1* shows the donor and receiver substrates, pressed together with a spacer between them, in the gas chamber with a laser pulse coming towards them; *Step 2* shows the sample during the transfer process; *Step 3* shows the removed receiver substrate after the transfer

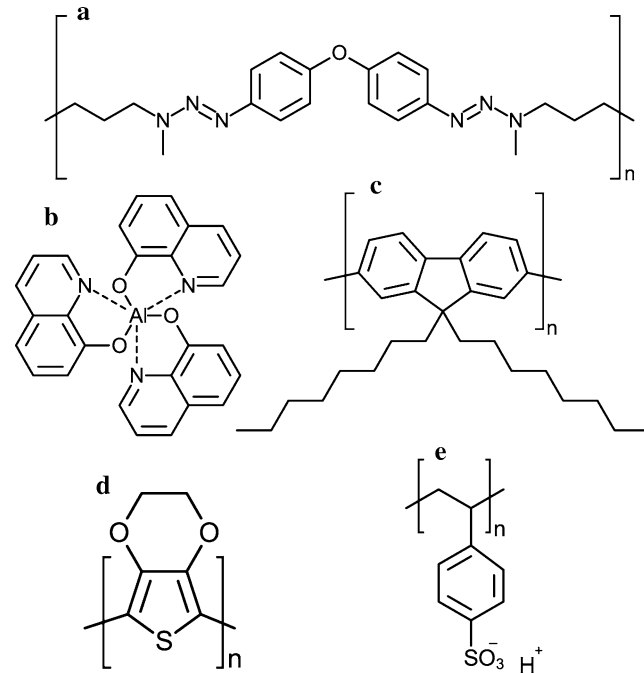


Fig. 2 The organic materials’ chemical structures used in these experiments. (a) Is the triazene polymer used as the DRL; (b) is Alq₃, the small-molecule OLED material; (c) is PFO, the blue-emitting polymeric OLED material; (d) is PEDOT; and (e) is PSS. (a)–(c) Were used on the donor substrate, and a blend of (d) and (e) was used on the receiver substrate

2 Experimental

2.1 Sample preparation

High-quality Suprasil fused silica substrates ($25 \times 25 \times 1 \text{ mm}^3$) have been used for the donor substrates, and plain glass microscope slides ($\sim 25 \times 25 \times 1 \text{ mm}^3$) have been used for the receiver substrates. Both substrates were cleaned in a series of ultrasonic baths: acetone, ethanol, alkali surfactant (HellmanexTM, Hellma AG), and water. The donor substrates were additionally cleaned using a UV–ozone cleaner before final bathing in microfiltered water. The receiver substrates were next coated with PEDOT:PSS (poly[3,4-ethylenedioxythiophene] blended with poly[styrenesulfonate]). The PEDOT:PSS (Clevios^{TMP} Al4083) was spin coated at 6000 rpm to give a film 30 nm thick. The chemical structures for PEDOT and PSS are shown in Fig. 2d and e.

The triazene polymer (TP) used here (Fig. 2a) was synthesized according to the procedure outlined before for TP-6a [23, 24]. The triazene polymer was dissolved in cyclohexanone:chlorobenzene solution at varying concentrations of up to 5 wt%. The donor substrates were spin coated with triazene polymer and the thicknesses measured using an Ambios XP-1 profilometer. The Ag layer was then evaporated onto the TP. For the initial atmospheric pressure measurements, thick Ag layers (200 nm) were used to try to increase the mechanical stability of the flyer. For the donor substrates transferred onto the PFO/PEDOT:PSS receiver substrates, a 150 nm Ag layer was used. For the samples used in the reduced pressure experiments, an 80 nm Ag layer was used. The thicknesses were measured in-situ using a quartz crystal microbalance. On top of the Ag, either 80 nm Alq₃ was evaporated or 80 nm PFO was spin coated from a toluene:p-xylene (1:1 wt) solution (15 mg/ml, 1500 rpm). The Alq₃ was bought from Sigma Aldrich (sublimed grade) and the PFO from American Dye Source. The chemical structures for Alq₃ and PFO are shown in Fig. 2b and c.

2.2 Experimental setup

The donor and receiver samples were placed together carefully, with the spacer in between, at one side of the pair, as illustrated in Fig. 3. This geometry was inspired by a previous study looking at the effect of optical standing waves on LIFT [25]. From all four corners of the substrate holder a uniform pressure was applied by screws with sprung ball bearings.

The laser used in these experiments is a 308 nm XeCl excimer laser. The beam was shaped into a square using a $2 \times 2 \text{ mm}^2$ square aperture, and the image of the mask was demagnified using a single achromat lens ($f = 250 \text{ mm}$) to

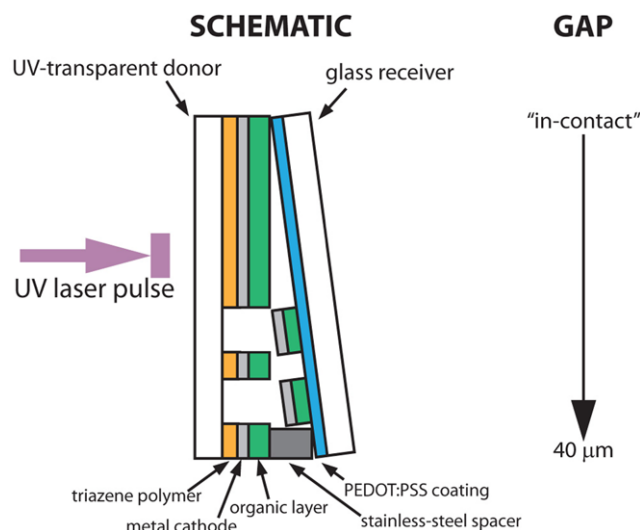


Fig. 3 A schematic showing how the substrate–substrate gap width was varied linearly across the sample. Based on a paper by Banks et al. [25]

give a square beam, $0.5 \times 0.5 \text{ mm}^2$, on the receiver substrate. Figure 1 shows the geometry of the sample with respect to the laser beam and gas chamber. The laser fluence was measured using a pyroelectric energy meter.

A gas chamber was specially constructed for the LIFT requirements, and contains a UV-transparent fused silica glass window for the laser beam, illustrated in Fig. 1, as well as three other windows for observation. The stage used to move the samples is a piezo-electric x – z stage with a rotation motor in the x – y plane. A dry roughing pump was attached to the chamber giving a maximum vacuum pressure of $2 \times 10^{-2} \text{ mbar}$. The pressure was measured using a standard pressure gauge.

The transfers onto the receiver substrates were characterized using light microscopy. All of the light microscopy images, except Fig. 6, were taken using top illumination on a Zeiss Axioplan instrument. Figure 6 was taken using back illumination on a Zeiss Axiovert instrument. The sensors were color balanced before taking the photographs, and the photographs are shown unmodified, except to combine photographs. Scanning electron microscopy (SEM, Hitachi S-4800) was also used to look at the surface at higher magnification.

2.3 Measuring the gap width

The substrate–substrate gap distance was measured using a Vis–IR absorption spectrometer (Varian Cary 500). Using a technique derived from published literature [26], the gap width can be found from the interference pattern in the absorption spectrum. An absorption spectrum in the range 800–2100 nm was acquired through both substrates, held together in a sample holder in the same way as for LIFT experiments. It is very simple to calculate the gap width from

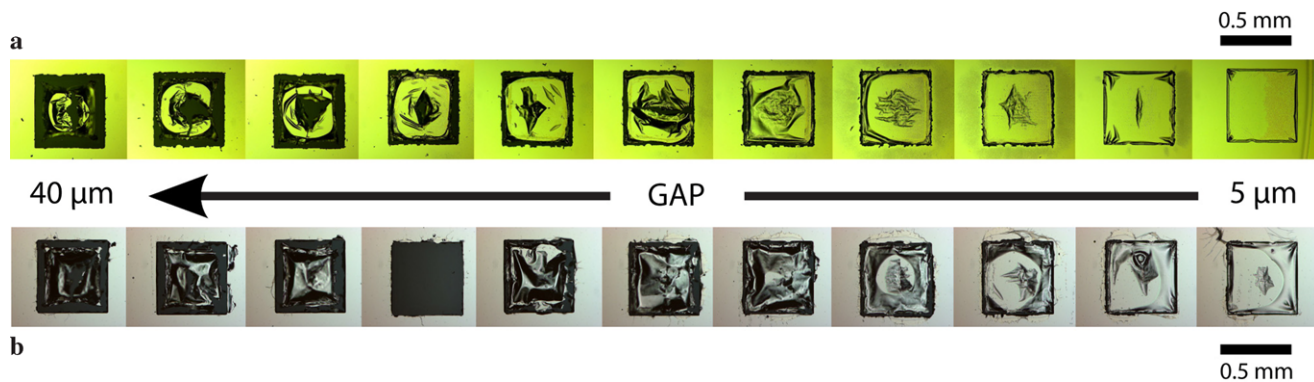


Fig. 4 Light microscopy images of the donor substrates consisting of fused silica/190 nm TP/200 nm Ag/ (a) 80 nm Alq₃ or (b) 80 nm PFO. The flyers are in the middle of the ablation spot after back-side

ablation with a fluence of 70 mJ/cm², with a linearly varying gap to the receiver substrate (glass/30 nm PEDOT:PSS)

the interference in these spectra, assuming the refractive index of air to be 1. Using this method, the gap width for the samples ‘in contact’ was calculated to be 2–3 μm, but was easily increased to >10 μm with small amounts of dust contamination.

To try and control the gap width, stainless steel with well-defined thickness (Brütsch Rüegger) was cut into the right shape for the sample holder. A variation in gap width across the sample was achieved by adding the spacer at one side, as shown in Fig. 3. However, because of the limitations of the size of the light beam for the absorption spectrometer, measurements of the gap width along the gradient could not be made. The gap width can only be measured for a constant gap width. To measure the variation in gap width in Fig. 3, the gap was measured with the spacer in and then an assumption of a linear gap gradient is made between the spacer and the ‘in-contact’ edge. At atmospheric pressure, the spacer used was 40 μm, and transfers were carried out across the whole sample, i.e. from a gap width of 40 μm to ‘in contact’. Because of the travel-distance limitations of the piezoelectric stage in the gas chamber (~7 mm maximum), a 100 μm spacer was used, and the transfers started 3/5th of the way across the sample from the spacer, allowing for approximately the same range of gap widths as the atmospheric pressure experiments: about 40 to 5 μm.

3 Results

3.1 Effect of adding a gap

The initial transfers at atmospheric pressure were done using donor substrates with a thick (200 nm) Ag layer. The main advantage of using a thicker layer was to prevent the flyer from fragmenting, which it does fairly easily at atmospheric pressure. The triazene DRL thickness was constant at 190 ± 10 nm for these experiments. The setup yielded a

matrix of attempted transfers with decreasing gap, from left to right, and increasing fluence, down the sample.

The transfer material will be referred to as a flyer when it is still on the donor substrate, and a pixel when it is deposited on the receiver substrate. It must be emphasized that for both Alq₃- and PFO-coated donor substrates the threshold fluence for ejection without a receiver substrate is around 50 mJ/cm². Attempted transfers of Alq₃ onto a receiver substrate resulted in almost no pixel deposition. The donor substrate for Alq₃ is shown in Fig. 4a, for ablation at a fluence of 70 mJ/cm², with the gap increasing from right to left. As the gap increases, the size of the flyer starts to shrink, and a hole also appears in the middle. The hole only really starts at a minimum gap distance of ~20 μm, at about the same time as the flyer starts to get noticeably smaller. It appears that the flyer is smaller at larger gap distances because the edges fold up, particularly in the corners.

Except for the organic layer material, Fig. 4b (PFO) shows the same donor substrate as Fig. 4a (Alq₃). PFO shows a similar trend to that observed for Alq₃, but there is less clearly defined flyer contact with the donor substrate. For the flyers between 5 and 20 μm gap the trend looks very similar, but above 20 μm the flyers appear more distorted. Overall, the area in contact with the donor substrate is less clear for PFO than for Alq₃, and the edges are not folded in the same uniform fashion as for Alq₃. For the fourth ablation crater from the left, at a gap width of 25–30 μm, the flyer is not present, indicating that a pixel has been deposited on the receiver substrate, which has indeed been observed (see Fig. 5, pixel circled in red).

Figure 5 shows the receiver substrate with pixels transferred from the 200 nm Ag/80 nm PFO donor substrate from Fig. 4b. The corresponding Ag/Alq₃ pixels were not transferred as successfully. The transferred Ag/PFO pixels clearly have a hole in the middle of them, and have a shape akin to a holed doughnut. At fluences greater than 86 mJ/cm², no pixel transfer was observed. The optimal fluence is around 80 mJ/cm².

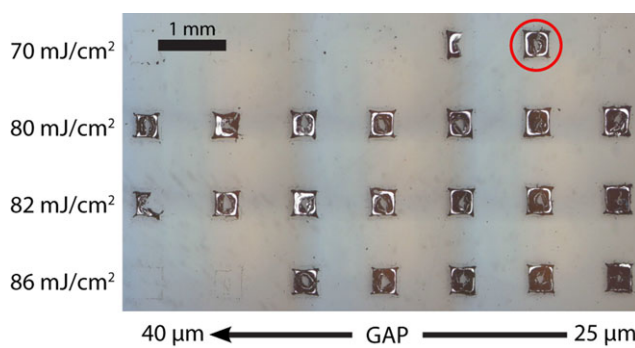


Fig. 5 Light microscopy images of the receiver substrate for the 190 nm TP/200 nm Ag/80 nm PFO donor substrate where transfer was achieved, but of non-functional pixels. A distinctive *doughnut* shape to the transferred pixels can be observed. The edges of the pixel, and the hole in the middle, are in contact with the substrate

3.2 Effect of modifying the receiver substrate

It was observed in a recent study that the receiver substrate can play a significant role in the transfer [17]. This observation suggested that adhesion between the flyer and the receiver substrate was a large part of the influence of the receiver substrate. Following on from these observations, in this study the receiver substrate has been modified by adding the organic material that is being transferred from the donor substrate (PFO in Fig. 6) onto the receiver substrate. For Alq₃, this proved to make very little difference, but the observations for PFO were interesting.

Figure 6 shows two different receiver substrates for the same donor substrate. Figure 6a shows an ordinary glass/PEDOT:PSS receiver substrate with the red rectangle corresponding approximately to the same fluence and gap window as Fig. 5. Figure 6b shows the same receiver substrate, but coated with an additional 80 nm PFO layer. The addition of PFO onto the receiver substrate clearly improves the likelihood of the transfer at smaller gaps and higher fluences (green rectangle). In addition, the pixels have a better shape at smaller gaps, <20 μm, without the hole in the middle, and a sharper square frame.

Whilst the transfer at 20–40 μm in Fig. 6a, shown in the red rectangle, is not quite as good as that observed in Fig. 5, the pattern is the same, with most of the successful transfers at gaps of 20–40 μm. These results for 150 and 200 nm Ag can also be compared with a comparable receiver substrate for 80 nm Ag in Fig. 7a, with the relevant fluence and gap range again in a red rectangle. These images show a distinct trend in terms of the influence of the metal layer thickness on the success rate of transferring these PFO pixels. In Fig. 5, the Ag layer of the donor substrate was 200 nm thick, in Fig. 6a it was 150 nm thick, and in Fig. 7a it was 80 nm thick. This shows that the thicker the Ag layer is, the better the chance of successful pixel deposition at gaps of 20–40 μm. However, it cannot be said that

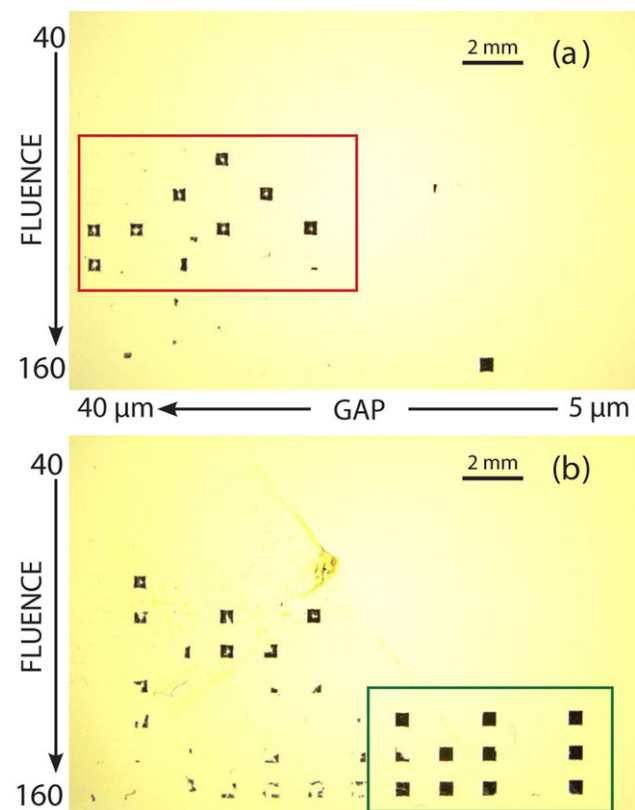


Fig. 6 Microscopy images of receiver substrates of PFO transfers, back illuminated. The donor substrate for both was 190 nm TP/150 nm Ag/80 nm PFO. (a) Is an ordinary receiver substrate, glass coated with 30 nm PEDOT:PSS, and (b) is the same as (a), but with 80 nm PFO spin coated onto the PEDOT:PSS. Fluences are in mJ/cm^2

the transfer is altogether successful, even in Fig. 5, given the *doughnut* shape of the pixels, which would almost certainly make non-functional devices. The pixels at low gaps and high fluences in Fig. 6b may make functional devices, but the use of PFO on both the receiver and donor substrates is not the goal in terms of PLED device architecture.

3.3 Effect of pressure reduction

Despite some successes with the PFO transfer across a gap in ambient conditions, it is clear that most of the deposited pixels would not be functional. For this reason, the environmental pressure in the gas chamber was reduced from 1 bar (atmospheric pressure) to 3×10^{-2} mbar. The samples for these experiments were the same as those used before, except that only 80 nm Ag was used. Thinner silver films were used to highlight the improvement in transfer quality because thinner metal films show noticeably poorer transfer at atmospheric pressure: see the red box in Fig. 7a compared to Fig. 5 and the red box in Fig. 6a.

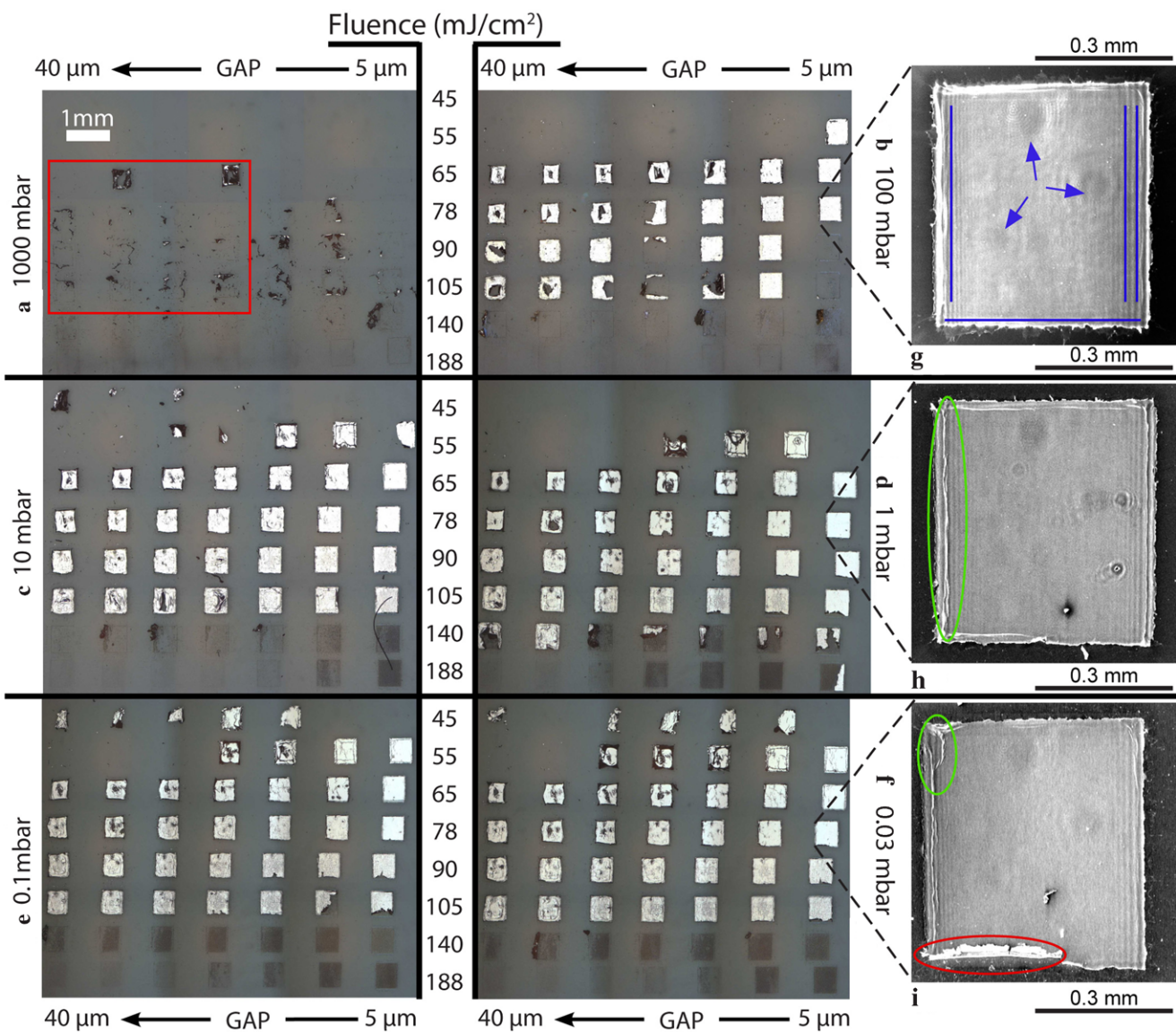


Fig. 7 Light microscopy and SEM images of the PEDOT:PSS-coated glass receiver substrates for 190 nm TP/80 nm Ag/80 nm PFO donor substrates with different environmental pressures. (a) Is atmospheric pressure (1000 mbar), and each subsequent picture from (b) to (f) is

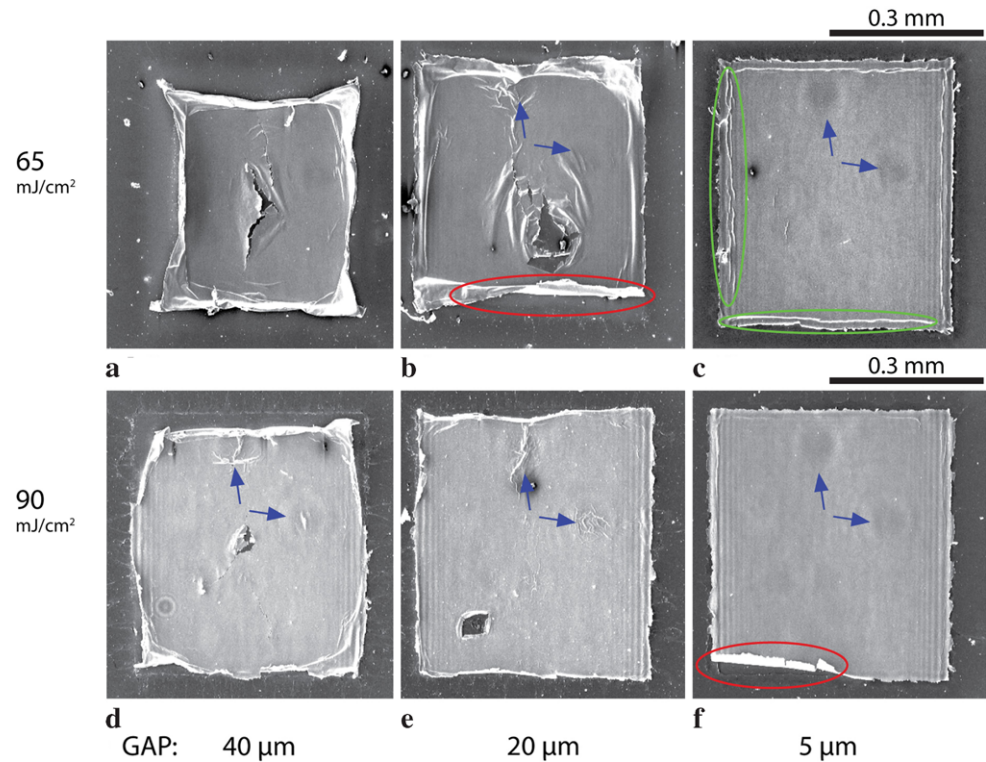
one order of magnitude lower. The fluence goes down from *top to bottom*, and the gap increases, from 5 to 40 μm , from *right to left*. Figures (g) to (i) are SEM images of the pixel at $\sim 5 \mu\text{m}$ gap distance and 78 mJ/cm^2 , for: (g) 100 mbar, (h) 1 mbar, and (i) 0.03 mbar

3.3.1 Pressure improvement

Figure 7 shows the large improvement of pixel transfer at reduced pressures. At 100 mbar (Fig. 7b) the transfer is already greatly improved and, below 10 mbar (Fig. 7c–f), the transfer is even better, but does not obviously improve with further pressure reduction. There is a degree of variation from sample to sample, but this is negligible, and probably dependent on the long-term variation in laser energy ($\sim 5\%$). In addition, the standard deviation of the fluence varied by $\pm 5\%$ from pulse-to-pulse instability. Nevertheless, the pressure trend is fairly clear, and the transfer consistency below 10 mbar is obvious: rows 3–6 (from top) are all completely

transferred for all of Fig. 7c–f, 10–0.3 mbar. The close-up SEM images, Fig. 7g–i, show three main observations. Firstly, there is folding just inside the edges. The folding is more pronounced at lower fluences, e.g. the single lines parallel to the pixel edges for pixels transferred at 55 mJ/cm^2 in Fig. 7c–f. They are particularly prominent within the pixel at low fluences and gap distances (an example is shown with a green ellipse in Fig. 7h). Secondly, irregular ripping of the metal along the edges can be clearly seen. Figure 8 suggests that the metal ripping is partly fluence dependent. An additional rip/fold is shown in a red ellipse in Fig. 7i to highlight a characteristic feature that appears after a subsequent transfer close enough to damage the pixel which has already

Fig. 8 SEM images of individual pixels transferred at two different fluences and three different gap distances at a pressure of 1 mbar (see Fig. 7d). (a) to (c) are at 65 mJ/cm^2 , and (d) and (e) are at 90 mJ/cm^2



been deposited, i.e. it is not a consequence of the original transfer. In Fig. 7i the chronology of the transfers goes from top to bottom; hence, the transfer in line 5 of Fig. 7d, at 90 mJ/cm^2 , would affect the line above where the pixel in Fig. 7i came from. The precise mechanism for this post-depositional effect is not clear, but is possibly the acoustic shock wave from the TP decomposition products. Lastly, a striped pattern can be observed parallel to the edges, particularly the right- and left-hand edges. This pattern has been highlighted in Fig. 7g with blue lines. Supplementary to this last observation are circles which appear to be embedded in the same way, as a topographical variation, indicated with blue arrows in Fig. 7g.

Figure 8 shows some SEM images of pixels transferred at 1 mbar. The pixels in the first row were transferred at a laser fluence of 65 mJ/cm^2 and those in the second row were transferred at a laser fluence of 90 mJ/cm^2 . The gap distances for the pixels are shown below the images. As well as the folding within the pixel in Fig. 8c (green ellipses), the folding of the edges is far more pronounced in pixels transferred over a larger gap (Fig. 8a and b). The overall effect of the folding is to shrink the pixel, similar to the observation for the Alq₃ flyers in ambient pressure in Fig. 4a. The pixels transferred at higher fluence, 90 mJ/cm^2 , do not show such pronounced folding. However, some curling up of the pixel edges is clear in Fig. 8d. The folding shown in a red ellipse is post-depositional damage caused by subsequent transfers, as explained in the previous paragraph for the pixel in Fig. 7i. The folding/curling-up observations from Fig. 8

match the shape of the flyers observed in shadowgraphic investigations at reduced pressure [19]. The shadowgrams in that paper showed that the flyer edges curled towards the donor substrate, the same direction as the folding in these SEM observations of pixels transferred at reduced pressure.

An additional observation from the SEM images is the regularity of the topological patterns, other than the folding. These patterns are hard to interpret and it is not clear what they are exactly. The stripes along the edges highlighted by blue lines in Fig. 7g are clearly present in some of the pixels in Fig. 8. The circular patterns indicated with blue arrows in Fig. 7g are also clearly present in some of the pixels in Fig. 8, too. The circular patterns appear to be located in the same places of the pixel, irrespective of the sample and pressure. Without additional research it is hard to interpret these patterns, but similar oscillatory patterns have been observed in front-side ablation of triazene before [27, 28].

3.3.2 Triazene DRL thickness comparison

In addition to the pressure and substrate–substrate gap dependence, the effect of changing the triazene DRL thickness was also investigated. The two extremes for successful transfer of 300 and 100 nm are shown in Fig. 9. The only TP film thinner than 100 nm that we investigated, 40 nm, did not appear to give any successful transfers, and we did not investigate thicknesses above 300 nm. Figure 9 shows the big difference in transfer success for 100 nm and 300 nm

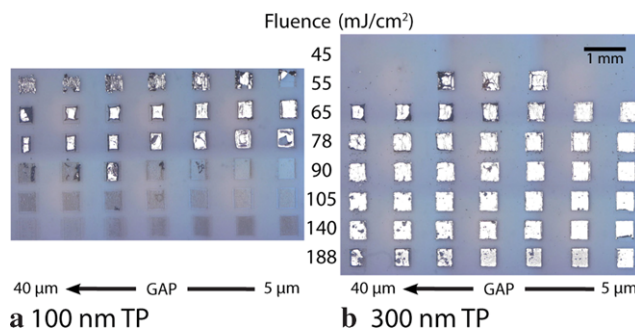


Fig. 9 Light microscopy images of the PEDOT:PSS-coated receiver substrates for TP/80 nm Ag/80 nm PFO donor substrate transfers at a range of fluences and gap distances. The pressure is 1 mbar. (a) Is for a donor substrate TP DRL thickness of 100 nm and (b) is for a donor substrate TP DRL thickness of 300 nm

TP at 1 mbar, with varying gap distance, as a function of fluence. Successful transfer is obtained above 140 mJ/cm² for 300 nm TP DRL, in Fig. 9b, whereas the flyer has been completely disintegrated by 90 mJ/cm² for 100 nm TP DRL. From front-side-ablation depth measurements of TP, a single 308 nm pulse of 60 mJ/cm² is enough to ablate 100 nm TP. More than 150 mJ/cm² is required to ablate 300 nm TP [29]. This explains the general trend of successful transfer at higher fluences for a greater TP DRL thickness.

4 Discussion

It has been proposed that the shock wave may play a significant role in affecting the quality of transfer [17]. In an earlier paper, reduced pressure environments were also investigated to try and remove the effect of the shock wave [19]. That investigation used time-resolved shadowgraphy to observe the flyer velocity and morphology, and to observe transfers over gaps of 0.5 and 1 mm. Although air resistance was clearly reduced, folding at low fluences and high impact at high fluences meant that transfer was unsuccessful over these big gap widths. It was actually concluded that transfer was better at atmospheric pressure with gaps of 0.5 and 1 mm [19].

In this study, Fig. 4 shows some of the best evidence for the power of the shock wave pushing back the flyer onto the donor substrate. For the Alq₃ donor substrates (Fig. 4a) the flyers at the larger gap distances (>20 μm) show a very interesting morphology. The edges of the flyer curl up, but an almost circular area of the flyer shows flat, uniform contact with the donor substrate. In the middle, a small hole appears like a hole punched through the flyer, resulting in a *doughnut* shape. The area of the flyer in contact with the donor substrate appears pressed down by the shock wave, and the edges which curl up are where the shock wave/air resistance force has dissipated enough to be too weak to push the flyer back onto the donor substrate. This effect should increase dramatically with gap distance, and indeed Fig. 4a

shows this. Although not shown, a deposit is left on the receiver substrate, which indicates that the flyer comes in contact, or at least close to contact, with the receiver substrate before being pushed back onto the donor substrate. Figure 4b does not show the same uniform contact with the donor substrate as Fig. 4a, presumably because of the different material properties of the organic PFO layer vs the Alq₃ layer. The polymeric PFO should have better film cohesion than the small-molecule Alq₃, and may well be more adhesive as well, particularly to another polymeric material (PEDOT:PSS). Due to the better PFO adhesion, transfer is expected to be better in atmosphere compared with Alq₃ films (Fig. 5). It may also explain why the PFO flyers are more folded and dishevelled in Fig. 4b than the Alq₃ flyers in Fig. 4a, because the adhesive force between the flyer and the PEDOT:PSS receiver is closer to the force exerted by the shock wave pushing the flyer back towards the donor substrate for PFO than for Alq₃.

The improvement in transfer from the addition of the PFO layer onto the receiver substrate, shown in Fig. 6, backs up the hypothesis that the adhesive force between the PFO and the PEDOT:PSS is only just below that of the force preventing transfer. The PFO was added onto the receiver substrate with the expectation that it will have a higher adhesion to the PFO flyers than PEDOT:PSS. A significant increase in transfer success is achieved at smaller gaps with the PFO on the receiver substrate. Previously, we observed that the addition of PEDOT:PSS greatly improved transfer of MEH-PPV ‘in contact’ at low fluences [17]. This result further increases the evidence for the effect of the receiver substrate upon the quality of transfer. However, it is important to note that the improvement may not be entirely due to adhesion, despite the hypothesis. The mechanical properties of the films may play a big role in dissipating energy in either the shock waves in the gas or from the impact of the flyer. This could also affect the quality of transfer.

Our understanding of the transfer process has been aided by the control of the gap width on the μm scale. Onto plain PEDOT:PSS-coated substrates, the PFO transferred much better across gaps >20 μm at atmospheric pressure, as shown in Fig. 5. In contrast, MEH-PPV (not shown, but used in previous investigations [9, 17]) was observed to transfer onto PEDOT:PSS well with a gap <10 μm. This explains why some degree of inconsistency was observed with MEH-PPV OLEDs ‘in contact’, as light contamination of dust particles increases the gap from ‘in contact’ to >10 μm. At reduced pressure good transfer appears more consistent, covering a larger range of fluences and gaps (Figs. 7 and 8). The morphology of the transferred pixel is greatly dependent on gap width, with significant folding observed even above 20 μm at lower fluences in Fig. 7. The reason that the transferred pixel shrinks as the gap width increases is probably because of the gaseous products of the triazene decomposition pushing their way around the edges of the pixel, as

observed in earlier shadowgraphy studies [19]. The larger the gap, the more this process is allowed to develop, and the more folded the flyer will be. However, this process is also fluence dependent, as shown in Fig. 8. Increasing the fluence will decrease the amount of folding, but at the cost of ablating more of the transfer material.

The transfer improvement by reducing the pressure is significant, as shown in Fig. 7. At atmospheric pressure, Fig. 7a, transfer of these thin films was very variable and difficult. At reduced pressures, the transfer is far more reliable and creates higher quality pixels, demonstrating the benefit of removing the air resistance and the shock wave, which are both proportional to pressure. In a previous study, the energy in the shock wave was calculated as a function of fluence [18]. In that article, the shock wave energy was calculated to be 30–40% of the input laser energy. The flyer kinetic energy was calculated to be ~3–4%, one order of magnitude lower. As the pressure is reduced, the shock wave energy is reduced. The shock wave energy is directly proportional to the gas density, i.e. pressure. Therefore, a single order of magnitude reduction in pressure brings the energy of the shock wave to the same order of magnitude as the flyer. As has been observed, reducing the shock wave energy increases the flyer energy [19]. This means that at ~100 mbar, the flyer energy will start to be above the shock wave energy, and transfer can be relied upon. Following this hypothesis, it would be expected that below 10 mbar no improvement in the transfer quality would be observed because the energy of the shock wave should already be at least one order of magnitude less than the flyer kinetic energy. The hypothesis is thus backed up by our observations.

A feature common to quite a lot of the data presented here is the hole in the middle of the pixels creating the *doughnut* pixels. This is primarily evident in the atmospheric pressure transfers with gaps above 20 μm , in Figs. 4 and 5. A minor hole is also seen in lower fluence pixels with large gap widths at reduced pressures, in Fig. 8. The origin of the hole must be because the center of the pixel will experience the maximum shear stress, but at least two mechanisms must be in play because of dual effects of higher pressure and greater gap width, as well as the less significant effect of lower fluence, all contributing to increasing the likelihood and size of holes in the center of the pixels. It must be considered that larger gaps mean that the flyer is in flight for a longer time, allowing heterogeneities to be accentuated. Higher air pressures also slow down the pixel, but additionally have air resistance and an acoustic shock wave affecting the flyer morphology.

A trend in the influence of the metal layer thickness is shown by Figs. 5, 6a, and 7a. The thicker the Ag metal layer, the better the likelihood of transfer at gaps >20 μm and at atmospheric pressure. Figure 5 uses an Ag layer of 200 nm, Fig. 6a an Ag layer of 150 nm, and Fig. 7a an Ag

layer of 80 nm. Two possible (but by no means exclusive) reasons for this trend are, firstly, that a thicker layer is mechanically stronger and, secondly, that a thicker layer gives the flyer more momentum to overcome air resistance and the reflected shock wave energy.

From front-side-ablation studies, it is known that around 80 mJ/cm² is required to fully ablate 190 nm TP [28, 29]. This means that the triazene may not be completely decomposed until a fluence of up to 80 mJ/cm², and possibly even above it. However, for this method of making OLEDs, with the relatively inert cathode already attached, this problem is irrelevant. What is clear, though, is that transfer can be achieved above the fluence where all the triazene is expected to be ablated (see Fig. 9a). All of the samples in this study used Ag as the metal but, when aluminium is used, the flyer can be transferred at even higher fluences [17]. Figure 9 also shows a minimum range of TP DRL thicknesses that can be chosen, from 100 to 300 nm.

Despite the vast improvement in transfer quality at reduced pressures and small gap widths, the SEM images clearly show further problems: ripples, irregular tearing at the edge of the flyers, and folding at lower fluences. Additionally, as mentioned before, a non-decomposed TP film may be left on the back of flyer, particularly at lower fluences. This study was done using silver as the metal transfer layer, but aluminium is a little more stable, with less evidence of rippling, tearing, and folding at the same fluences as silver. This highlights the importance of the material choices for both the donor and the receiver. For every given system, a full optimization will need to take place, which will be easier for some materials than for others.

5 Summary

Three main observations have been made. Firstly, the increase of the substrate–substrate gap distance affects the morphology of the transferred pixel by reducing the flyer size via folding. Secondly, transfer of PFO-coated donor substrates could be improved in atmosphere by coating the receiver substrate with PFO. Thirdly, reducing the pressure dramatically improves the success rate and pixel morphology quality of the transfer. A comparison of transfer quality for different TP DRL thicknesses has been carried out, and it has been concluded that a minimum thickness of 100 nm is required for successful transfer. Above this, the DRL thickness was picked so that most of the TP would be ablated at the transfer fluence. In the case of 80 nm Ag/80 nm PFO this thickness is 150–200 nm. In addition, thicker Ag cathode layers are shown to improve the likelihood of transfer and pixel quality at atmospheric pressure.

In conclusion, to optimize the pressure and gap distance for ~100 nm Ag/~100 nm PFO donor substrates, the fol-

lowing conditions are needed: a gap less than μm , a pressure below 100 mbar, a fluence of 50–100 mJ/cm^2 , and a TP thickness greater than 100 nm. These results show the feasibility of transfer of the first functional OLED devices over a known gap width, permitting side-by-side transfer more easily. LIFT is still by no means universal, but reducing the pressure and controlling the gap width will extend the range of thin-film materials that can be deposited using LIFT. By reducing the pressure we have shown that LIFT with controlled substrate–substrate gaps as large as 30 μm can deposit, onto a PEDOT:PSS/glass receiver substrate, 500 μm^2 pixels of metal/organic material bilayer thin films, with a good morphology quality.

Acknowledgements Funding for this research was provided by the EU, via the e-LIFT project, and the Swiss National Science Foundation. The authors would like to thank Parul Dhagat (Empa) for reviewing the manuscript.

References

1. M.L. Levene, R.D. Scott, B.W. Siryj, *Appl. Opt.* **9**(10), 2260–2265 (1970)
2. J. Bohandy, B.F. Kim, F.J. Adrian, *J. Appl. Phys.* **60**(4), 1538–1539 (1986)
3. W.A. Tolbert, I.-Y. Sandy Lee, M.M. Doxtader, E.W. Ellis, D.D. Dlott, *J. Imaging Sci. Technol.* **37**, 411–421 (1993)
4. C. Arnold, P. Serra, A. Piqué, *Mater. Res. Soc. Bull.* **32**, 23–31 (2007)
5. J.A. Barron, R. Rosen, J. Jones-Meehan, B.J. Spargo, S. Belkin, B.R. Ringeisen, *Biosens. Bioelectron.* **20**(2), 246–252 (2004)
6. A. Doraiswamy, R. Narayan, T. Lippert, L. Urech, A. Wokaun, M. Nagel, B. Hopp, M. Dinescu, R. Modi, R. Auyeung, D. Chrisey, *Appl. Surf. Sci.* **252**, 4743–4747 (2006)
7. M. Duocastella, J. Fernández-Pradas, J. Domínguez, P. Serra, J. Morenza, *Appl. Phys. A, Mater. Sci. Process.* **93**(4), 941–945 (2008)
8. J. Xu, J. Liu, D. Cui, M. Gerhold, A.Y. Wang, M. Nagel, T.K. Lippert, *Nanotechnology* **18**(2), 025403 (2007)
9. R. Fardel, M. Nagel, F. Nüesch, T. Lippert, A. Wokaun, *Appl. Phys. Lett.* **91**, 061103 (2007)
10. L. Rapp, A.K. Diallo, A.-P. Alloncle, C. Videlot-Ackermann, F. Fages, P. Delaporte, *Appl. Phys. Lett.* **95**(17), 171109 (2009)
11. D.P. Banks, K. Kaur, R. Gazia, R. Fardel, M. Nagel, T. Lippert, R.W. Eason, *Europhys. Lett.* **83**(3), 38003 (2008)
12. J. Wang, R.C.Y. Auyeung, H. Kim, N.A. Charipar, A. Piqué, *Adv. Mater.* **22**(40), 4462–4466 (2010)
13. A. Palla-Papavlu, V. Dinca, I. Paraico, A. Moldovan, J. Shaw-Stewart, C.W. Schneider, E. Kovacs, T. Lippert, M. Dinescu, *J. Appl. Phys.* **108**(3), 033111 (2010)
14. V. Dinca, A. Palla-Papavlu, M. Dinescu, J. Shaw-Stewart, T. Lippert, F. Di Pietrantonio, D. Cannata, M. Benetti, E. Verona, *Appl. Phys. A, Mater. Sci. Process.* **101**(3), 559–565 (2010)
15. A. Palla-Papavlu, I. Paraico, J. Shaw-Stewart, V. Dinca, T. Savopol, E. Kovacs, T. Lippert, A. Wokaun, M. Dinescu, *Appl. Phys. A, Mater. Sci. Process.* **102**(3), 651–659 (2011)
16. N.T. Kattamis, N.D. McDaniel, S. Bernhard, C.B. Arnold, *Appl. Phys. Lett.* **94**(10), 3 (2009)
17. J. Shaw-Stewart, T. Lippert, M. Nagel, F. Nüesch, A. Wokaun, *ACS Appl. Mater. Interfaces* **3**(2), 309–316 (2011)
18. R. Fardel, M. Nagel, F. Nüesch, T. Lippert, A. Wokaun, *J. Phys. Chem. C* **113**(27), 11628–11633 (2009)
19. R. Fardel, M. Nagel, F. Nüesch, T. Lippert, A. Wokaun, *J. Phys. Chem. C* **114**(12), 5617–5636 (2010)
20. J. Shaw Stewart, R. Fardel, M. Nagel, P. Delaporte, L. Rapp, C. Cibert, A.-P. Alloncle, F. Nüesch, T. Lippert, A. Wokaun, *J. Optoelectron. Adv. Mater.* **12**(3), 605–609 (2010)
21. C.W. Tang, S.A. VanSlyke, *Appl. Phys. Lett.* **51**(12), 913–915 (1987)
22. S.-A. Chen, H.-H. Lu, C.-W. Huang, *Adv. Polym. Sci.* **212**, 49–84 (2008)
23. J. Stebani, O. Nuyken, T. Lippert, A. Wokaun, *Makromol. Chem., Rapid. Commun.* **14**, 365 (1993)
24. M. Nagel, R. Hany, T. Lippert, M. Molberg, F. Nüesch, D. Rentsch, *Macromol. Chem. Phys.* **208**, 277–286 (2007)
25. D.P. Banks, K. Kaur, R.W. Eason, *Appl. Opt.* **48**(11), 2058–2066 (2009)
26. R. Swanepoel, *J. Opt. Soc. Am. A* **2**(8), 1339–1343 (1985)
27. R. Fardel, M. Nagel, F. Nüesch, T. Lippert, A. Wokaun, B. Luk'yanchuk, *Appl. Phys. A, Mater. Sci. Process.* **90**(4), 661–667 (2008)
28. M. Nagel, R. Fardel, P. Feurer, M. Häberli, F. Nüesch, T. Lippert, A. Wokaun, *Appl. Phys. A, Mater. Sci. Process.* **92**(4), 781–789 (2008)
29. R. Fardel, P. Feurer, T. Lippert, M. Nagel, F. Nüesch, A. Wokaun, *Appl. Surf. Sci.* **254**, 1332–1337 (2007)